Determination of seasonal variations in the Martian neutral atmosphere from observations of ionospheric peak height

Hong Zou,[1,2] Robert J. Lillis,[2] Jin Song Wang,[3] and Erling Nielsen[4]

Received 17 March 2011; revised 3 June 2011; accepted 9 June 2011; published 15 September 2011.

[1] Radio occultation experiments allow us to measure electron and neutral densities in planetary atmospheres. Here we investigate such measurements from the Mars Global Surveyor Radio Science experiment in 2 consecutive Martian years (25 and 26). Using Chapman theory, we parameterize the ionospheric peak altitude in terms of the solar zenith angle, neutral scale height at the peak, neutral density at 20 km and the effective neutral scale height ($\overline{\xi}_n$) between 20 km and the peak, finding the latter to be the primary driver of peak altitude. From the occultation data, we observe that altitudes of peak electron density at high northern latitudes show a clear seasonal trend, increasing from northern summer (Ls = 90°) to northern autumn (Ls = 180°), driven by substantial increases in $\overline{\xi}_n$, despite neutral densities at 20 km steadily decreasing as surface temperatures drop. We find these trends to be consistent with neutral density predictions from the LMD Mars Global Circulation Model at both 20 km and 130 km. The primary mechanism responsible for this increase in the 20–130 km effective neutral scale height (and hence temperature) is the southward drift in subsolar latitude as northern summer becomes autumn. This drives the seasonal evolution of the Martian interhemispheric Hadley circulation. The downward branch of this circulation leads to an increasing warming in the middle atmosphere at high north latitudes from the northern summer to the northern autumn, causing an increase in neutral scale height at and below the ionospheric peak and thus an increase in the ionospheric peak height.

Citation: Zou, H., R. J. Lillis, J. S. Wang, and E. Nielsen (2011), Determination of seasonal variations in the Martian neutral atmosphere from observations of ionospheric peak height, *J. Geophys. Res.*, *116*, E09004, doi:10.1029/2011JE003833.

1. Introduction

[2] The Martian ionosphere has been explored by radio occultation experiments onboard several spacecraft. Many aspects of the Martian dayside ionosphere, particularly properties of the electron density maximum (hereafter referred to as the peak), can be explained by simple Chapman theory. The dependences of the peak electron density on solar radiation [*Stewart and Hanson*, 1982; *Breus et al.*, 2004; *Zou et al.*, 2006; *Fox and Yeager*, 2009; *Withers*, 2009], solar zenith angle [*Hantsch and Bauer*, 1990; *Zhang et al.*, 1990; *Gurnett et al.*, 2005; *Fox and Yeager*, 2009; *Withers*, 2009], and solar cycle [*Bauer and Hantsch*, 1989] generally agree with the expectation for a Chapman layer-like ionosphere. Effects from other influences, such as magnetic field [*Krymskii et al.*, 1995, 2002, 2003, 2004; *Breus et al.*, 2004; *Nielsen et al.*, 2007; *Zou et al.*, 2010], are left for approaches other than Chapman theory.

[3] The peak height of the Martian ionosphere is a function of Solar Zenith Angle (SZA) because it corresponds to a slant optical thickness of unity. The peak, herein, refers to the main peak of the Martian ionosphere, which is produced by the photoionization in the ~150–1000 Å wavelength range [*Fox and Yeager*, 2006]. The peak height h_m increases with increasing SZA, which can be described by: $h_m = h_{m0} + H \ln [\sec (\mathrm{SZA})]$ where h_{m0} is the peak height at the subsolar point and H is the atmospheric scale height. *Hantsch and Bauer* [1990] used Viking Orbiter Radio Science data to find that h_{m0} and H equal approximately 120 km and 10 km respectively. Besides SZA, the neutral atmosphere is another main controller of the Martian ionosphere [*Withers*, 2009]. The longitudinal variation in the peak height found by the Mars Global Surveyor Radio Science (MGS/RS) experiment is consistent with zonal variations found in neutral density measurements [*Bougher et al.*, 2001, 2004]. Thermal tides modulate the neutral density, which results in the longitude variation of the peak height [*Withers et al.*, 2003; *Cahoy et al.*, 2006, 2007]. However, tides are not the only atmospheric processes that affect the peak height. According to the radio occultation measurements from Mariner 9, the peak

[1]Institute of Space Physics and Applied Technology, School of Earth and Space Sciences, Peking University, Beijing, China.
[2]Space Science Laboratory, University of California, Berkeley, California, USA.
[3]National Center for Space Weather, China Meteorological Administration, Beijing, China.
[4]Max Planck Institute for Solar System Research, Katlenburg-Lindau, Germany.

0148-0227/11/2011JE003833

height was 20–30 km higher than usual when a global dust storm was subsiding [*Hantsch and Bauer*, 1990], i.e., when the lower atmosphere had expanded substantially [*Wang and Nielsen*, 2004].

[4] There are still aspects of the Martian ionosphere which are not fully understood and need further investigation. One example is seasonal variation of the Martian ionosphere, which has been studied with the Mars Thermospheric Global Circulation Model (MTGCM) [*Bougher et al.*, 1990, 2000, 2001] and with the Mars Advanced Radar for Subsurface and Ionospheric Sounding (MARSIS) on Mars Express in the solar longitude ranges near the solstices [*Morgan et al.*, 2008]. The asymmetry of the Martian ionospheric peak height between two hemispheres was also studied with measurements by the MGS/RS experiment in a narrow solar longitude range (~134°–146°) [*Zou et al.*, 2005]. However, long-term continuous measurements of the Martian ionosphere have never been used to study the seasonal variations. The accessible observation with the longest continuous time coverage for the same hemisphere made by MGS is less than two Martian seasons [*Hinson*, 2008a; *Withers et al.*, 2008]: the longest solar longitude coverage of those measurements is around 100° or approximately a quarter Martian year from the northern summer (Ls = 70°–90°) to the northern autumn (Ls = 180°–200°).

[5] In this paper, we investigate long-term ionospheric and neutral density measurements in the Martian northern hemisphere from the MGS/RS experiment. In section 2, two long-term ionospheric data sets from MGS/RS experiment are introduced to show the variations of the key parameters of the Martian ionosphere at the peak. In section 3, Chapman theory is used to analyze the controllers of the peak height of the Martian ionosphere. In section 4, neutral density in the lower atmosphere as measured by MGS/RS is investigated as one of the main controllers of the ionospheric peak height. In section 5 we derive some neutral atmospheric parameters from these ionospheric and atmospheric data. Section 6 compares parameters derived from MGS/RS data with simulations of the neutral atmospheric parameters by the LMDMGCM (Laboratoire de Météorologie Dynamique Mars Global Circulation Model). In section 7, the possible reasons for the seasonal variation of these neutral atmospheric parameters are discussed. Finally, a summary is presented in section 8.

2. Ionospheric Measurements by the MGS/RS Experiment

[6] All MGS/RS electron density profiles of the Martian ionosphere are available at the Planetary Data System (PDS) [*Hinson*, 2008a]. Among these measurements, two long time periods of observation (EDS1: November 2000 to June 2001 MY 25 with 1572 profiles and EDS2: November 2002 to June 2003 MY 26 with 1806 profiles) are used in this investigation. Both data sets were measured in high latitude regions of the northern hemisphere (60°–90°N). The measurements provide altitude profiles of electron densities larger than $\sim 10^3$ cm^{-3} [*Hinson et al.*, 1999]. To make sure the main peak of the Martian ionosphere in the photochemical equilibrium region, the data with SZA < 85° are selected [*Fox and Yeager*, 2006].

[7] According to *Breus et al.* [2004], the electron density profile near the main peak of the Martian ionosphere can be approximated by a Taylor series. The electron density n as function of altitude h can be written as follows:

$$n(h) = a + bh + ch^2, \tag{1}$$

which is sufficiently accurate within the altitude interval $|h - h_{peak}| \le H_n(h_{peak})/2$; ($h_{peak}$ is the peak height, $H_n(h_{peak})$ is the neutral scale height at the main peak and the altitude interval used in this study is 20 km around h_{peak}). Assuming the validity of Chapman theory (including photochemical equilibrium), the coefficients in equation (1) can be described as

$$a = n_{peak}\left(1 - \frac{h_{peak}^2}{4H_n^2(peak)}\right) \quad b = \frac{n_{peak}h_{peak}}{2H_n^2(peak)} \quad c = -\frac{n_{peak}}{4H_n^2(peak)}, \tag{2}$$

where n_{peak}, h_{peak} and $H_n(peak)$ are peak electron density, peak height and the neutral scale height at the peak height respectively. With equations (1) and (2), the main peak height and the neutral scale height near the peak can be estimated from each electron density profile.

[8] Figure 1 shows the derived main peak heights of the Martian ionosphere, the neutral scale heights near the peak, the local time, longitude and latitude for these two data sets, as a function of solar longitude. Figure 1 (left) displays data from EDS1 (Ls: 70 ~ 180°), while Figure 1 (right) displays data from EDS2 (Ls: 90 ~ 200°). As can be seen, these two data sets were collected at high northern latitudes from the northern summer to the northern autumn (Ls = 90° is northern summer solstice, 180° is northern autumnal equinox). The SZA of the two data sets decreases at first, reaches the minimum at the solar longitude around 140–150° and then increases. The SZA variation of the peak height can clearly be seen. However, the peak heights in northern autumn (after Ls = 160°) seem to be on average larger than that in the northern summer at similar SZAs.

[9] The SZA variations of the two data sets and the associated orbit parameters are shown in Figure 2. Daily averages are plotted to minimize the longitudinal effect. Each data set can be separated into two groups by the minimum SZA. The group with the decreasing SZA is called the summer data and denoted by the dots in Figure 2, while the group with the increasing SZA is called the autumn data and denoted by the plusses. It is clear that the peak heights of the autumn data are higher on average than that of the summer data at the same SZA for both EDS1 and EDS2. The possible reasons for this increase in the peak height include the latitude, local time and solar longitude variation of the Martian ionosphere. The third row of Figure 2 shows that the variation in latitude for a given SZA is quite small (no more than 7°). In any case, autumn data latitudes are generally higher than summer data latitudes for EDS1, whereas the opposite is true for EDS2. Therefore the increase in the peak height does not likely much depend on the latitude variation of the data. According to the fourth row of Figure 2, the local time differences between the autumn and summer data are about 4 h (EDS1) and 10 h (EDS2). So the local time and solar longitude variation are the most plausible reasons for the increase in the peak height.

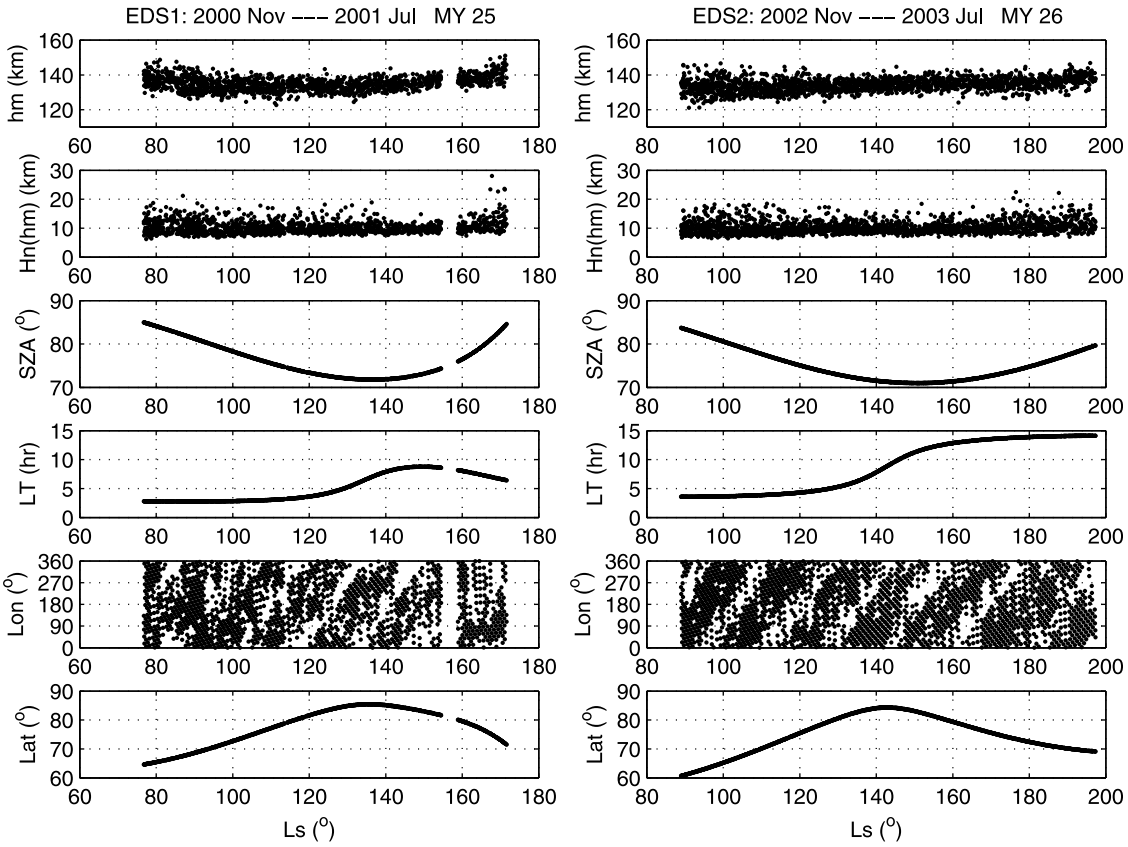

Figure 1. The solar longitude variations of the 2 data sets: EDS1 and EDS2. The left column displays data of EDS1 as function of solar longitude (Ls: 70 ~ 180°). The right column displays data of EDS2 as function of solar longitude (Ls: 90 ~ 200°). The first row shows the variation of the main peak height (h_m), the second shows the variation of the neutral scale height near the peak ($H_n(h_m)$). The lower panels show the solar zenith angle (SZA), local time (LT), longitude (lon) and latitude (lat) for each occultation respectively.

[10] In 3 section, Chapman theory is used to analyze the controllers of the peak height of the Martian ionosphere.

3. Theoretical Considerations

[11] It is known that near the region of main maximum electron density, the Martian ionosphere is in photochemical equilibrium [*Hantsch and Bauer*, 1990]. *Breus et al.* [2004] verified that even if the neutral scale height above the peak is not constant, the following equation should be approximately satisfied in the Martian ionosphere:

$$\sec\chi \cdot \sigma \cdot N_{co_2}(h_m) \cdot H_n(h_m) \approx 1, \tag{3}$$

where χ is the SZA, σ the mean EUV radiation absorption cross section, $Nco_2(h_m)$ and $H_n(h_m)$ the density and scale height of the neutral atmosphere (mainly CO_2) at the ionospheric peak, respectively. It should be noted that a similar expression is obtained in the frame of classical Chapman theory only under the assumption of a constant neutral scale height above the main ionospheric peak [*Budden*, 1966]. The CO_2 density at the peak can be described as

$$N_{co_2}(h_m) = N_0 \exp\left(-\int_{h_0}^{h_m} \frac{dh}{\xi_n(h)}\right), \tag{4}$$

where N_0 is the CO_2 density at a reference height (h_0), ξ_n is the scale height of the CO_2 number density, a function of height. If we substitute $Nco_2(h_m)$ in equation (3) with equation (4) and take the logarithm, then we obtain

$$\int_{h_0}^{h_m} \frac{dh}{\xi_n(h)} = \ln[\sec\chi \cdot \sigma \cdot N_0 \cdot H_n(h_m)]. \tag{5}$$

[12] Since the neutral density scale height is not a constant in the Martian atmosphere, the first mean value theorem for integration [*Zwillinger*, 1992] is applied to equation (5) and yields

$$\frac{(h_m - h_0)}{\overline{\xi}_n} = \ln[\sec\chi \cdot \sigma \cdot N_0 \cdot H_n(h_m)], \tag{6}$$

where $\overline{\xi}_n$ is the effective mean neutral density scale height between the reference height and the ionospheric peak height. The peak height of the Martian ionosphere can then be described as

$$h_m = h_0 + \overline{\xi}_n \cdot \ln[\sec\chi \cdot \sigma \cdot N_0 \cdot H_n(h_m)]. \tag{7}$$

It can be seen that h_m is a function of χ, N_0, $H_n(h_m)$ and $\overline{\xi}_n$. Except for χ, the variables N_0, $H_n(h_m)$ and $\overline{\xi}_n$ are parameters

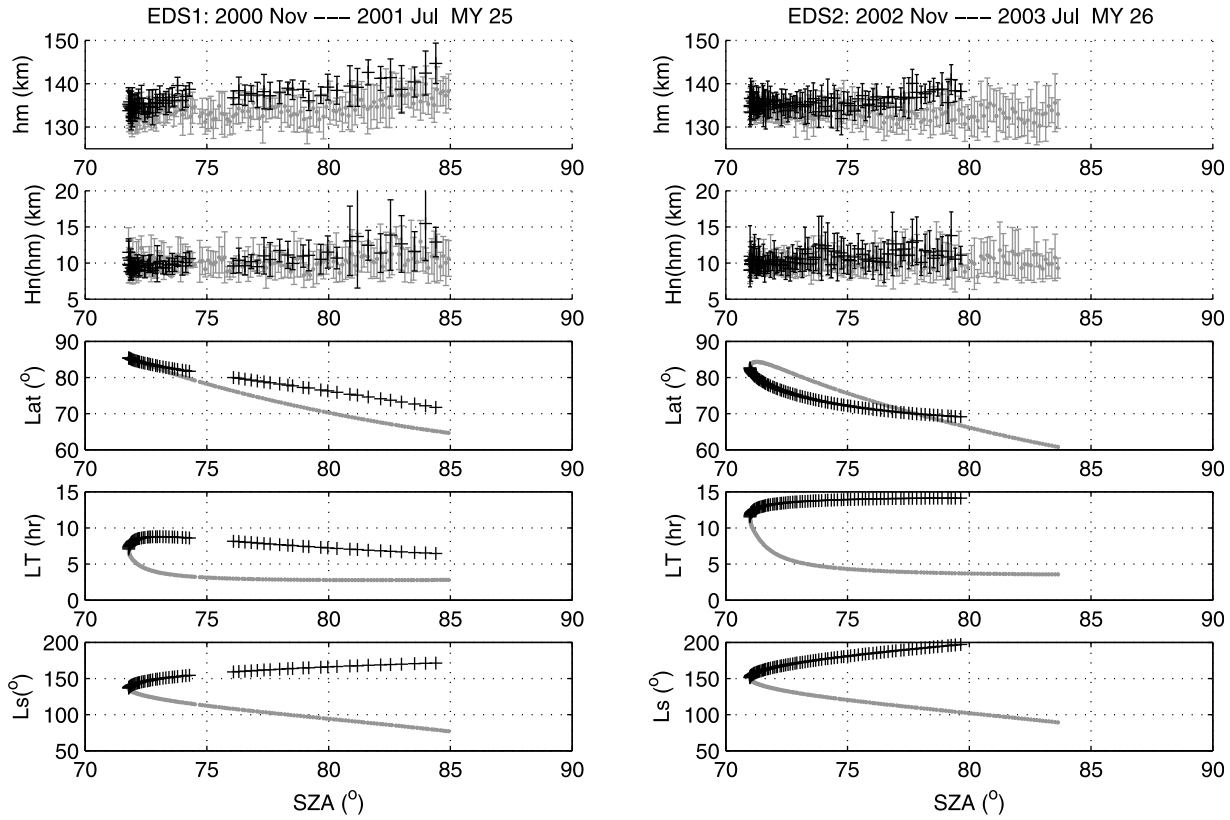

Figure 2. The SZA variations of (left) EDS1 and (right) EDS2. The first row shows the main peak heights; the second row shows the neutral scale heights near the peak; the third row shows the local times (LT); the fourth row shows the latitudes (Lat) and the fifth row shows the solar longitudes (Ls). The gray dots show the data before the minimum SZA and the black plusses show the data after the minimum SZA. The error bars show the standard deviations.

of the neutral atmosphere. Therefore, it is verified that the neutral atmosphere and solar zenith angle be the main controllers of the peak height of the Martian ionosphere.

[13] In section 4, the lower Martian atmosphere is investigated to check the correlation between the variation of lower Martian atmosphere and that of ionospheric peak height.

4. Atmospheric Measurements by the MGS/RS Experiment

[14] As well as ionospheric retrievals, MGS/RS measurements also allow the retrieval of Martian neutral density profiles in the lower atmosphere up to ~50 km with a technique differs from the ionospheric measurements [*Fjeldbo et al.*, 1977; *Lindal et al.*, 1979; *Hinson et al.*, 1999]. The neutral atmospheric measurements of MGS/RS experiment are also available at the Planetary Data System (PDS) [*Hinson*, 2008b]. It is possible to derive N_0 in equation (7), i.e., the neutral (CO_2) density at a reference height (h_0), from the MGS/RS measurements. These data acquired over three Martian years (from 1998 to 2003, MY 24, 25, 26) in the high latitude (60°–90°) region of the northern hemisphere are used to investigate the neutral density variation of the lower atmosphere. According to *D. E. Smith et al.* [2001], the average planetocentric distance of the equipotential surface of the atmospheric data is 3376.1 ± 1.4 km in the same latitude range (60°–90°) of the northern hemisphere. To avoid possible violent density variations in the troposphere, the height of 20 km above the relative equipotential surface is chosen as the best reference height. Figure 3 shows the solar longitude variations of the retrieved neutral densities at the reference height and the corresponding local time in the high latitude (60°–90°) region of the northern hemisphere of Mars.

[15] According to Figure 3 (top), the high interannual repeatability of solar longitude variation of the neutral density at the reference height is obvious, which is in accord with the observations of the Thermal Emission Spectrometer (TES) on MGS [*Liu et al.*, 2003] and ground-based millimeter wave results of *Clancy et al.* [2000]. The neutral density reaches its maximum in the northern summer and then decreases to its minimum in the northern winter. In contrast, the ionospheric peak height shows the opposite variation from the northern summer to autumn. Therefore, according to equation (7), variation in $H_n(h_m)$ and $\overline{\xi}_n$ together must more than compensate for this decrease in N_0 to explain the increase in the ionospheric peak height from summer to autumn. Another feature of the annual variation of the neutral density at the reference height is the independence of local time. In Figure 3 (bottom), the neutral densities in the year of 2001 (MY 25) and 2003 (MY 26) are close near the northern autumn equinox

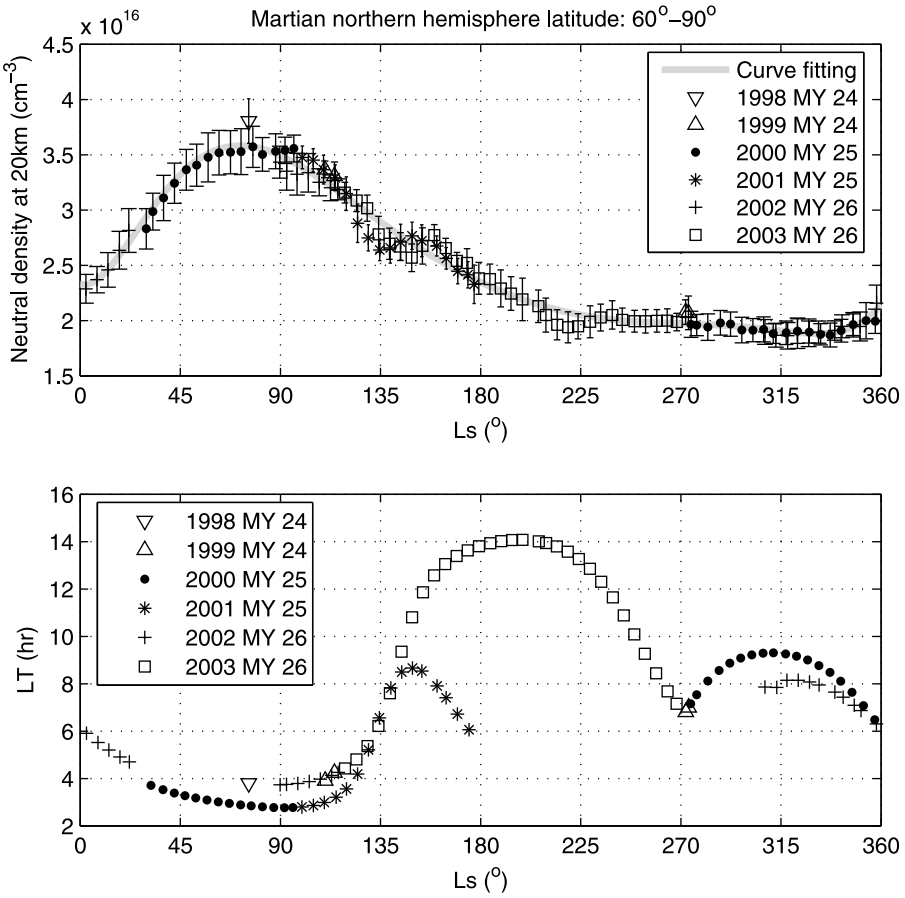

Figure 3. (top) The 5 degree running averaged solar longitude variations of the neutral density at 20 km above the equipotential surface and (bottom) corresponding local time in the high latitude (60°–90°) region of the northern hemisphere of Mars during three Martian years (from 1998 to 2003). The different symbols show the data in different years. The solid line in Figure 3 (top) shows the curve of a polynomial fit to the neutral density variation. The error bars show the standard deviations.

(Ls ~ 180°), while the corresponding local time difference is about 8 h.

[16] The local time variation of the upper atmosphere of Mars has been studied with the measurements by accelerometer [*Keating et al.*, 1998; Withers, 2006] and ultraviolet spectrometer (Spectroscopy for Investigation of Characteristics of the Atmosphere of Mars, SPICAM, onboard Mars Express) [*Forget et al.*, 2009] and simulated with Mars general circulation models [e.g., *Bougher et al.*, 1999; *González-Galindo et al.*, 2009]. The measurements and simulations both show a large local time variation in the upper atmosphere of Mars. So the local time cannot be excluded from the reasons for the increase in the ionospheric peak height.

[17] With the neutral density at 20 km shown in Figure 3, other parameters in equation (7) can be derived from the ionospheric data. The results are shown in section 5.

5. Evaluating Neutral Atmospheric Parameters From MGS/RS Ionospheric Measurements

[18] Among the parameters in equation (7), χ is known, h_m and $H_n(h_m)$ can be derived from the electron density profile by equation (1) and (2), the neutral density N_0 at the reference height h_0 can be evaluated from the polynomial fitting curve of the annual atmospheric density variation as shown in Figure 3 (top), while σ is considered to be a constant. So $\bar{\xi}_n$, the effective neutral scale height between the reference height and the ionospheric peak height for EDS1 and EDS2, can be determined from equation (7)

$$\bar{\xi}_n = \frac{h_m - h_0}{\ln[ch(\chi) \cdot N_0 \cdot H_n(h_m) \cdot \sigma]}. \tag{8}$$

In the calculation, the function $\sec(\chi)$ in equation (7) is substituted by the function $ch(\chi)$, Chapman's grazing incident function, which takes into account absorption of the solar radiation as it passes obliquely through the atmosphere [*Chapman*, 1931; *Titheridge*, 1988]. The mean ionization cross section, σ, is approximately 2.3×10^{-17} cm^2 [*Torr et al.*, 1979; *Wang and Nielsen*, 2003; *Zou et al.*, 2005]. Then with the known $\bar{\xi}_n$ and N_0, the neutral density at the ionospheric peak height can be calculated by

$$N(h_m) = N_0 \exp\left(-\frac{(h_m - h_0)}{\bar{\xi}_n}\right). \tag{9}$$

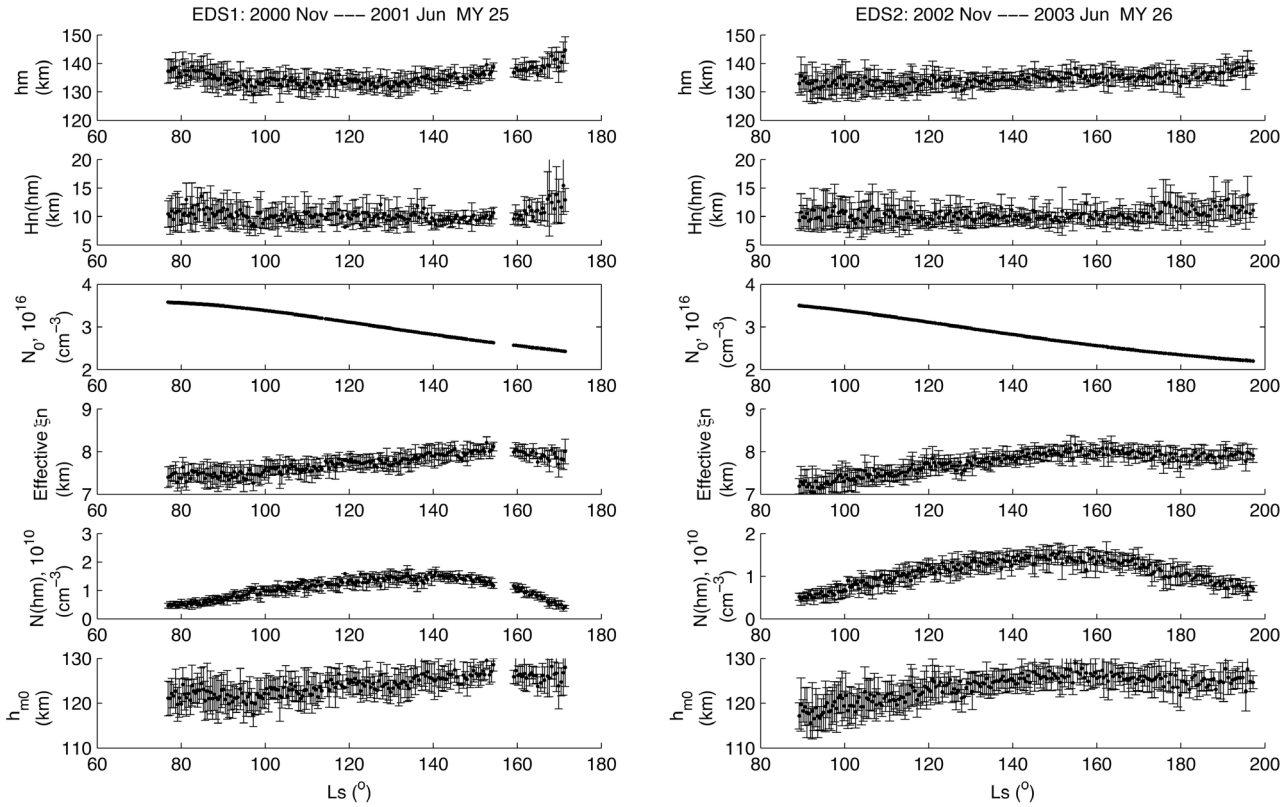

Figure 4. Solar longitude variations of atmospheric and ionospheric quantities calculated from MGS/RS data for (left) EDS1 and (right) EDS2. The first row shows the ionospheric peak heights; the second row shows the neutral scale heights near the peak; the third row shows the neutral densities at the reference height derived from the polynomial fitting for the annual variation of the neutral density measured by MGS/RS experiment in three Martian years as shown in Figure 3; the fourth row shows the effective neutral scale height calculated with equation (8); the fifth row shows the neutral density at the ionospheric peak height calculated with equation (9); the sixth row shows the subsolar peak height of the Martian ionosphere calculated from equation (10). The error bars show the standard deviations.

In order to compare the neutral atmospheric effect on the ionospheric peak height of Mars, the subsolar (SZA = 0°) peak heights, h_{m0}, for EDS1 and EDS2 can be derived from equation (7) as

$$h_{m0} = h_0 + \overline{\xi}_n \cdot \ln[N_0 \cdot H_n(h_m) \cdot \sigma]. \tag{10}$$

[19] Figure 4 shows the solar longitude variations of the effective neutral scale height $\overline{\xi}_n$, neutral density at the ionospheric peak height $H_n(\mathrm{h}_m)$ and the subsolar peak height h_m evaluated from the ionospheric and atmospheric measurements of MGS/RS experiment. It can be seen that the evaluated effective neutral scale height (Figure 4, third row) and subsolar peak height (Figure 4, fifth row) show a similar solar longitude variation, increasing from northern summer to northern autumn, while the evaluated neutral density at the ionospheric peak height (Figure 4, fourth row) shows a different solar longitude variation, increasing until Ls = 140°, then decreasing rapidly as northern autumn progresses.

[20] To know the main controller of the Martian ionospheric peak height, we now estimate the effects of χ, N_0, $H_n(h_m)$ and $\overline{\xi}_n$ on h_m. The partial differentials of h_m can show the effects of these parameters on the variation of $\mathrm{h_m}$,

$$\frac{\partial h_m}{\partial \chi} = \overline{\xi}_n \tan(\chi), \tag{11a}$$

$$\frac{\partial h_m}{\partial N_0} = \frac{\overline{\xi}_n}{N_0}, \tag{11b}$$

$$\frac{\partial h_m}{\partial H_n(h_m)} = \frac{\overline{\xi}_n}{H_n(h_m)}, \tag{11c}$$

$$\frac{\partial h_m}{\partial \overline{\xi}_n} = \ln[\sec\chi \cdot \sigma \cdot N_0 \cdot H_n(h_m)]. \tag{11d}$$

Suppose that there is a small variation in these parameters ($\Delta\chi$, $\Delta \mathrm{N_0}$, $\Delta\ \mathrm{H_n(h_m)}$, $\Delta\overline{\xi}_n$), and either causes a small variation in the ionospheric peak height ($\Delta h_m(\chi)$, $\Delta h_m(N_0)$,

Table 1. The Measured and Evaluated Parameters of the Martian Ionosphere and Atmosphere for EDS1 at Ls = 90° ± 2° and Ls = 160° ± 2°

Parameters	Value1 (Ls = 90° ± 2°)	Value2 (Ls = 160° ± 2°)	Difference between Value2 and Value1
h_m (km)	134.7 ± 1.1	137.6 ± 0.6	2.9 ± 1.3
h_{m0} (km)	121.5 ± 1.0	126.4 ± 0.5	4.9 ± 1.1
N_0 (cm^{-3})	$(3.49 \pm 0.01) \times 10^{16}$	$(2.56 \pm 0.01) \times 10^{16}$	$(-0.93 \pm 0.01) \times 10^{16}$
Hn(hm) (km)	10.7 ± 0.6	10.0 ± 0.6	−0.7 ± 0.8
$\bar{\xi}_n$ (km)	7.50 ± 0.06	8.00 ± 0.03	0.50 ± 0.07

$\Delta h_m(H_n(h_m))$, $\Delta h_m(\bar{\xi}_n)$), then equations (11a)–(11d) can be written as

$$\Delta h_m(\chi) = \bar{\xi}_n \cdot \chi \cdot \tan(\chi) \cdot \frac{\Delta\chi}{\chi}, \tag{12a}$$

$$\Delta h_m(N_0) = \bar{\xi}_n \cdot \frac{\Delta N_0}{N_0}, \tag{12b}$$

$$\Delta h_m(H_n(h_m)) = \bar{\xi}_n \cdot \frac{\Delta H_n(h_m)}{H_n(h_m)}, \tag{12c}$$

$$\Delta h_m(\bar{\xi}_n) = \bar{\xi}_n \cdot \ln[\sec\chi \cdot \sigma \cdot N_0 \cdot H_n(h_m)] \cdot \frac{\Delta\bar{\xi}_n}{\bar{\xi}_n} = \bar{\xi}_n \cdot \frac{h_m - h_0}{\bar{\xi}_n} \cdot \frac{\Delta\bar{\xi}_n}{\bar{\xi}_n}. \tag{12d}$$

Giving typical values of these parameters [e.g., *Bauer and Hantsch*, 1989] in equations (12a)–(12d), say, $H_n(h_m) \sim$ 10 km, $h_m \sim 130$ km, $\chi = 75°$, $\bar{\xi}_n \sim 8$ km and $h_0 \sim 20$ km above the equipotential surface, the ratio of the ionospheric peak height variations caused by these parameters can be evaluated as

$$\Delta h_m(\chi) : \Delta h_m(N_0) : \Delta h_m(H_n(h_m)) : \Delta h_m(\bar{\xi}_n) = 4.9\frac{\Delta\chi}{\chi} : \frac{\Delta N_0}{N_0} : \frac{\Delta H_n(h_m)}{H_n(h_m)} : 13.8\frac{\Delta\bar{\xi}_n}{\bar{\xi}_n}. \tag{13}$$

Now of course these 4 parameters do not typically show similar variations, but we feel it is instructive to show that, in the theoretical case where all four parameters have the same relative variation, the effects of N_0 and $H_n(h_m)$ are the same, the effect of χ overwhelms them, while the most important controller is $\bar{\xi}_n$.

[21] The measured and evaluated parameters of the Martian ionosphere and atmosphere for EDS1 at Ls = 90° ± 2° are compared with those at Ls = 160° ± 2°, as shown in Table 1. It can be seen that the derived subsolar peak height and the neutral scale height at the peak shown in Table 1 are consistent with the previous results reported by *Hantsch and Bauer* [1990].

[22] By applying equations (12a)–(12d) to the case of SZA = 0°, the differences in the subsolar ionospheric peak height, Δh_{m0}, caused by the variations of N_0, $H_n(h_m)$ and $\bar{\xi}_n$ between Ls = 90° and Ls = 160° are calculated as

$$\Delta h_{m0}(N_0) = \bar{\xi}_n \cdot \frac{\Delta N_0}{N_0} = 7.5 \times \frac{-0.93}{3.49} = -2.0 \text{ km},$$

$$\Delta h_{m0}(H_n(h_m)) = \bar{\xi}_n \cdot \frac{\Delta H_n(h_m)}{H_n(h_m)} = 7.5 \times \frac{-0.7}{10.7} = -0.5 \text{ km},$$

$$\Delta h_{m0}(\bar{\xi}_n) = \bar{\xi}_n \cdot \ln[\sec\chi \cdot \sigma \cdot N_0 \cdot H_n(h_m)] \cdot \frac{\Delta\bar{\xi}_n}{\bar{\xi}_n} = (134.7 - 20) \times \frac{0.5}{7.5} = 7.6 \text{ km}. \tag{14}$$

All these factors make a total difference in Δh_{m0} of about 5.1 km, which sufficiently explains the 4.9 km increase in h_{m0} evaluated from MGS/RS measurements. It can be seen from equation (14) that the increase in $\bar{\xi}_n$ overwhelms the negative effects of N_0 and $H_n(h_m)$ and causes an increase in the subsolar ionospheric peak height. Therefore the main controller of this increase in the ionospheric peak height is the variation of the effective neutral scale height between the reference height and the ionospheric peak height.

[23] Actually, the priority of the controllers of the subsolar ionospheric peak height is also determined by the choice of the reference height. For an extreme example, if the reference height is selected to be at the ionospheric peak height, $h_0 = h_m$, and $N_0 = N(h_m)$, then $\bar{\xi}_n$ equals $H_n(h_m)$, and equation (14) turns out to be

$$\Delta h_{m0}(N_0) = \bar{\xi}_n \cdot \frac{\Delta N_0}{N_0} = H_n(h_m) \cdot \frac{\Delta N(h_m)}{N(h_m)},$$

$$\Delta h_{m0}(H_n(h_m)) = \bar{\xi}_n \cdot \frac{\Delta H_n(h_m)}{H_n(h_m)} = H_n(h_m) \cdot \frac{\Delta H_n(h_m)}{H_n(h_m)},$$

$$\Delta h_{m0}(\bar{\xi}_n) = (h_m - h_0) \cdot \frac{\Delta\bar{\xi}_n}{\bar{\xi}_n} = 0. \tag{15}$$

It can be seen that for this extreme case, the priorities of the neutral density and neutral scale height are the same (the controller $\bar{\xi}_n$ becomes the controller $H_n(h_m)$). According to the MGS/RS measurements as shown in Table 1, the relative variation of the neutral density at the peak from Ls = 90° to Ls = 160°, is about 4 times larger than that of the neutral scale height at the peak, i.e., the neutral density becomes the main controller.

[24] Therefore as we increase the reference height, the effect of the effective neutral scale height on the ionospheric peak height decreases compared to that of the neutral density at the reference height.

[25] Now we would like to compare the variations of neutral atmosphere parameters derived from MGS/RS ionospheric data, with predictions from a global circulation model of the Martian atmosphere using the same orbital conditions.

6. Comparison With a Global Circulation Model of the Martian Atmosphere

[26] It is instructive to compare the neutral atmospheric parameters evaluated from the MGS/RS measurements, with those simulated with a global circulation model of the Martian atmosphere. This model is the France-based Laboratoire de Météorologie Dynamique Mars Global Circulation Model (LMD MGCM). The LMD MGCM model is a physics-based model of the Martian atmosphere from the ground up to the lower exosphere [*Forget et al.*, 1999; *Angelats i Coll et al.*, 2004].

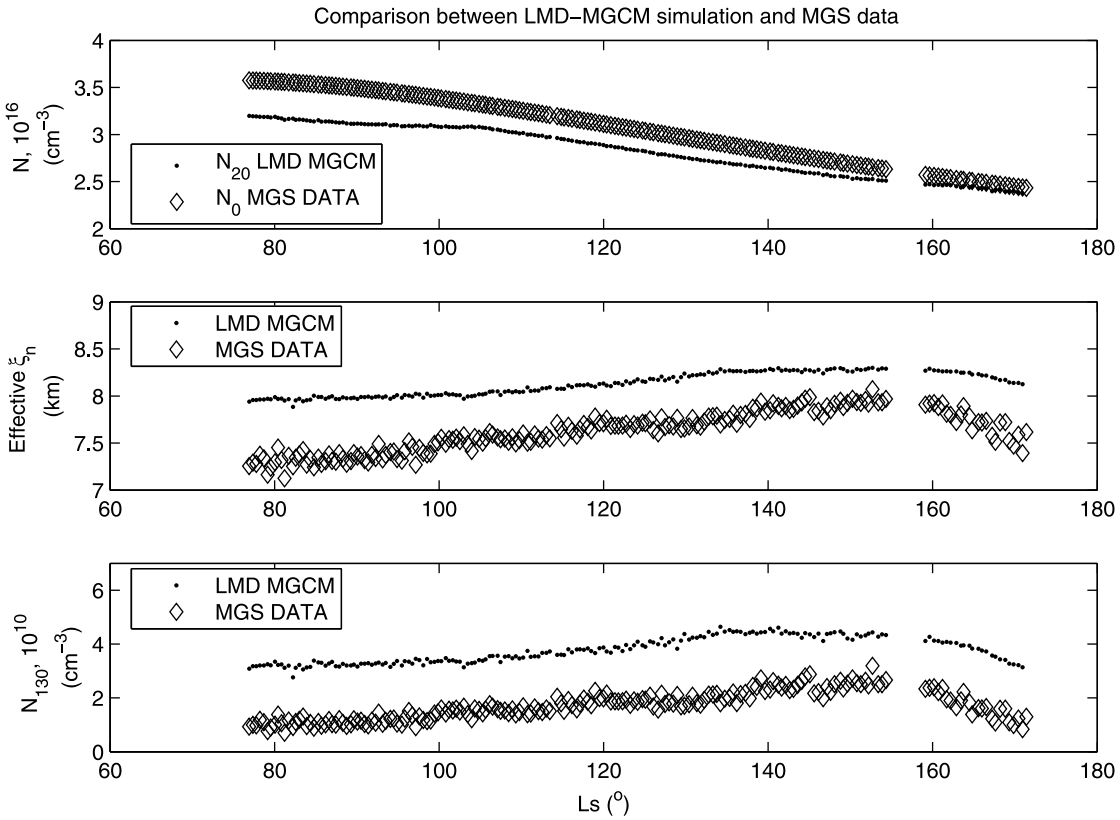

Figure 5. Comparison between the daily averaged solar longitude variations of the neutral atmospheric parameters simulated by the LMD MGCM model with the same longitudes, latitudes, local times and solar longitudes as EDS1 under the solar maximum condition and those derived from the MGS/RS measurements. The simulated neutral density is in the unit of kg/m^3. Supposing the mean molecular weight of the Martian atmosphere is 43.34 g/mol [*Seiff and Kirk*, 1976], the number neutral density can be calculated. The first and last panels show the neutral densities at 20 km ($N_{20\text{-}LMD}$ and N_0) and 130 km ($N_{130\text{-}LMD}$ and $N_{130\text{-}MGS}$) above the equipotential surface of Mars; the middle panel shows the derived effective neutral scale height between 20 km and 130 km ($\overline{\xi}_n$) by equation (15). The dots show the results estimated by the LMD MGCM model as denoted by LMD MGCM; the diamonds show the results derived from the MGS/RS measurements as denoted by MGS DATA.

[27] The LMD MGCM solves the primitive equations of hydrodynamics on a sphere, using a grid point discretization. The radiative balance accounts for the effect of CO_2 and suspended dust. A realistic CO_2 condensation scheme is included, essential for a good simulation of the surface pressure annual cycle. A water cycle [*Montmessin et al.*, 2004] and a photochemical model for the lower atmosphere [*Lefèvre et al.*, 2004] have also been included in the model. A number of subgrid scale processes near the surface are considered, in particular the boundary layer turbulence, convection, relief drag and gravity wave drag. Surface processes are accounted for by including MOLA topography and TES thermal inertia. In its current version, 14 chemical species are included in the model, undergoing transport by the general circulation, as well as molecular diffusion. N_2 and Ar are treated as chemically inert, while all the other species are affected by chemistry. For extension up to the thermosphere, parameterizations for the following physical processes are also included: NLTE corrections to the CO_2 IR radiative balance, UV heating, thermal conduction, molecular diffusion and a photochemical model appropriate for the upper atmosphere [*Angelats i Coll et al.*, 2005; *González-Galindo et al.*, 2005, 2009]. Densities from the LMD MGCM were retrieved using the Mars Climate Database [*Millour et al.*, 2008] (available at http://johnson.lmd.jussieu.fr:8080/las/servlets/dataset).

[28] Using the same orbit data (solar longitude, local time, latitude and longitude) of EDS1 (from 2000 November to 2001 June, MY 25), the neutral densities at 20 km and 130 km above the equipotential surface of Mars are calculated by the LMD MGCM model under solar maximum EUV conditions. The dust condition used in the model is taken from the average TES dust scenario from Mars year 24 [*Smith*, 2004]. The effective neutral scale height between 20 km and 130 km, $\overline{\xi}_{n-LMD}$, can be calculated by

$$\overline{\xi}_{n-LMD} = \frac{130\text{ km} - 20\text{ km}}{\ln(N_{20-LMD}) - \ln(N_{130-LMD})}, \tag{16}$$

where $N_{20\text{-}LMD}$ and $N_{130\text{-}LMD}$ are the simulated neutral densities at 20 km and 130 km. The solar longitude variations of these three Martian atmospheric parameters are shown in Figure 5.

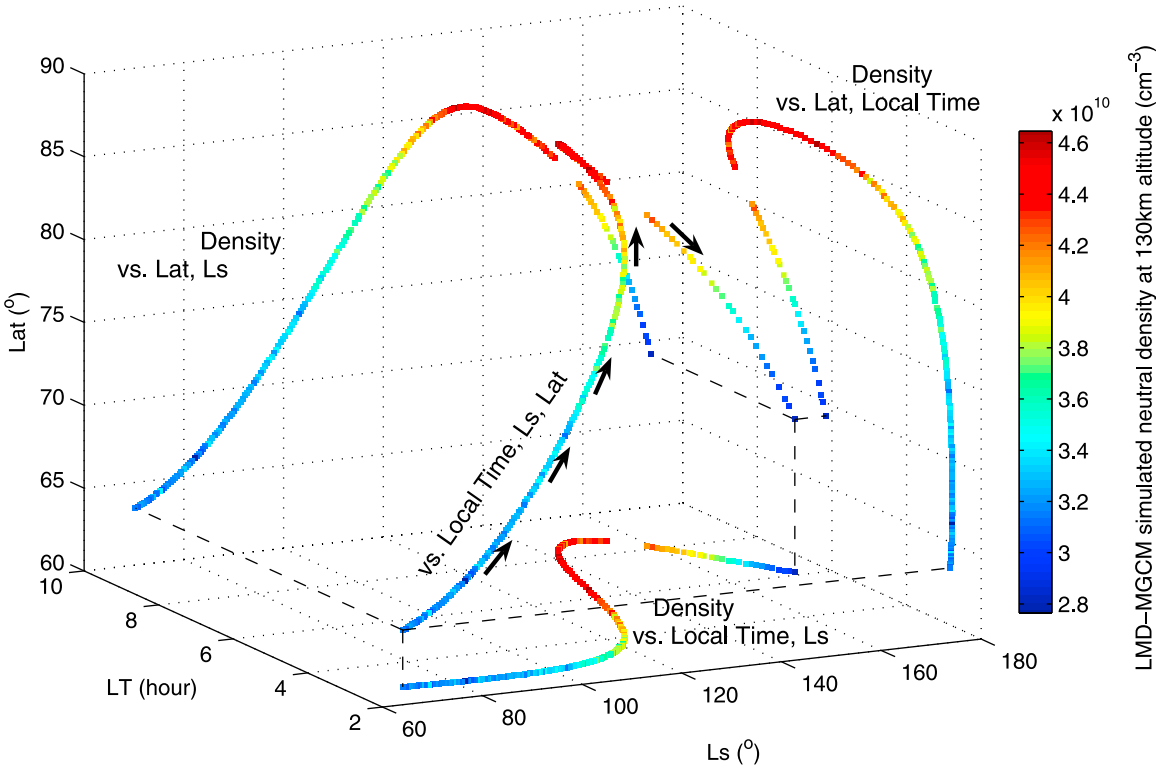

Figure 6. The latitude, local time and solar longitude variations in neutral density at 130 km estimated by the LMD MGCM model for the measurements in the EDS1 data set. The colors represent the neutral density variation in cm^{-3}.

[29] For comparison, the neutral atmospheric parameters derived from MGS/RS measurements are also shown in Figure 5. Assuming a constant scale height for the neutral atmosphere from 130 km to the ionospheric peak, the neutral density at the ionospheric peak height, $N(h_m)$, can be normalized to 130 km with

$$N_{130-MGS} = N(h_m) \cdot \exp\left(\frac{h_m - 130\ \text{km}}{H_n(h_m)}\right). \qquad (17)$$

[30] The solar longitude variation of the normalized neutral density at 130 km, $N_{130\text{-}MGS}$, is shown in Figure 5 (bottom). With the MGS/RS measurements, the effective neutral scale height between 20 km and 130 km, $\overline{\xi}_{n-MGS}$, can also be derived from the normalized neutral density at 130 km, $N_{130\text{-}MGS}$ and the curve fitted neutral density at 20 km, N_0, with equation (16). We can see that the neutral atmospheric parameters calculated by the LMD MGCM model match the MGS/RS measurements very well in terms of seasonal trend, though not quite as well in absolute value. The neutral density at 20 km simulated by the model is in close accord with the MGS/RS measurements, with the largest difference (<10%) appearing at Ls = ~70°. The simulated neutral density at 130 km ($N_{130\text{-}LMD}$) and the effective neutral scale height ($\overline{\xi}_{n-LMD}$) both increase modestly from Ls = 70° until ~150° before decreasing somewhat sharply, showing a similar solar longitude variation as those derived from the MGS/RS measurements. While the simulated $N_{130\text{-}LMD}$ and $\overline{\xi}_{n-LMD}$ are on average larger than $N_{130\text{-}MGS}$ and $\overline{\xi}_{n-MGS}$, these differences may be caused by the overestimation of the neutral density by the LMD MGCM model for the lower thermosphere (z < 130 km) [*Forget et al.*, 2009]. *Lillis et al.* [2010] also show an overestimation by the LMD MGCM when comparing with neutral mass densities at 185 km derived from electron reflectometry, where the simulation's overestimation was typically a factor of 2–6. Despite these differences, the simulation of the LMD MGCM model verifies that the increase of the effective neutral scale height from the northern summer to autumn is responsible for the observed increase in the ionospheric peak height. The possible reasons for the variation of the effective neutral scale height are discussed in section 7.

7. Discussion

[31] According to the theoretical analysis in section 3, the peak height of the Martian ionosphere is determined by neutral density at a reference height, neutral scale height near the peak, the effective neutral scale height below the peak and by the solar zenith angle.

[32] As stated in section 5, the increase in the ionospheric peak height measured by the MGS/RS experiment is mainly caused by the variation of the effective neutral scale height between the reference height and the ionospheric peak height. The simulation by the LMD MGCM model in section 6 reproduces similar trends to those derived from the MGS/RS experiment.

[33] From Figures 4 and 5, it can be seen that the effective neutral scale height increases from the northern summer to

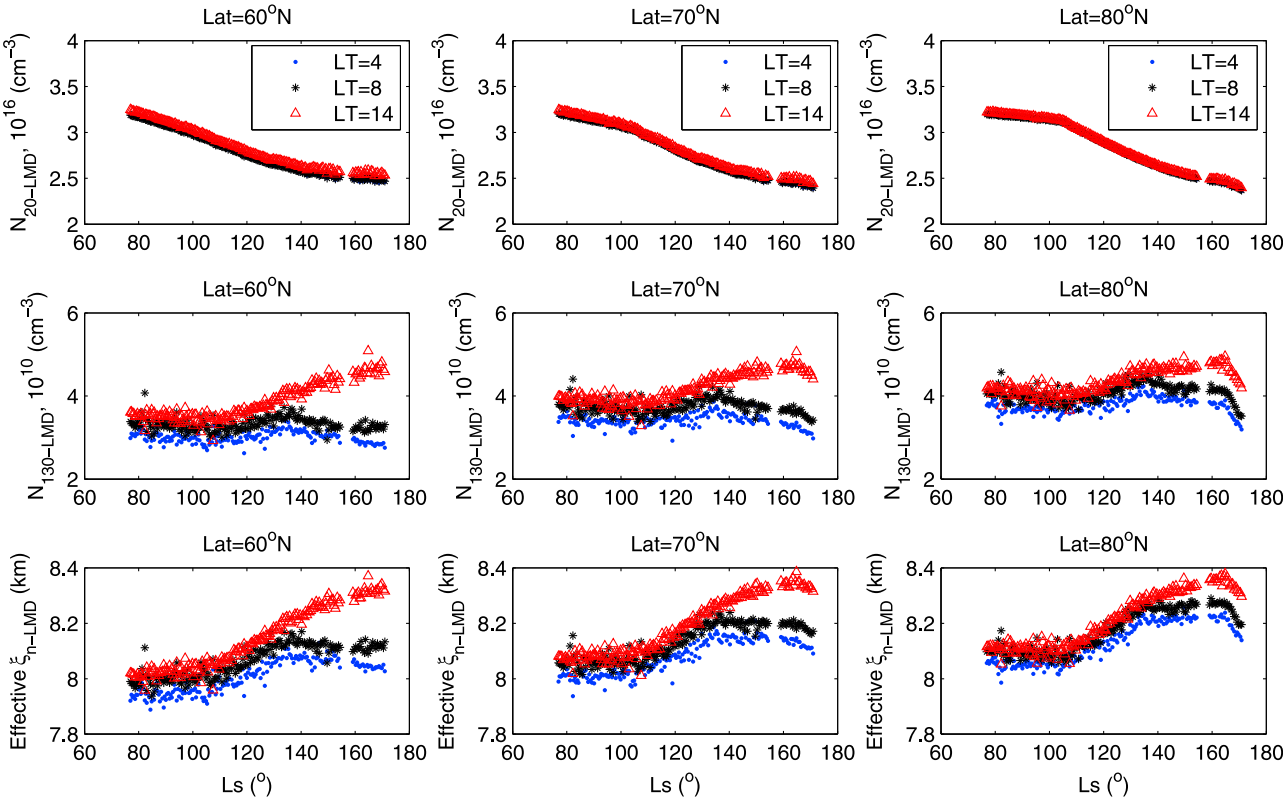

Figure 7. The daily averaged solar longitude variations of the neutral atmospheric parameters simulated by the LMD MGCM model at three local times (04:00, 08:00, 14:00) and at three latitudes (60°, 70°, 80°) with the same longitudes and solar longitudes as EDS1 under solar maximum conditions. (left) The simulation at Lat = 60°; (middle) the simulation at Lat = 70°; and (right) the simulation at Lat = 80°. (top and middle) the neutral densities at 20 km ($N_{20\text{-}LMD}$) and 130 km ($N_{130\text{-}LMD}$) above the equipotential surface of Mars; (bottom) the derived effective neutral scale height between 20 km and 130 km ($\overline{\xi}_{n-LMD}$) from equation (15). The points, stars, triangles show the simulations at LT = 04:00, 08:00, 14:00 h respectively.

the northern autumn. This increase in the effective neutral scale height contributes to an opposite solar longitude variation of the neutral density of the upper atmosphere (at the ionospheric peak height) from that of the lower atmosphere (at the reference height, 20 km) over the same period.

[34] As shown in Figures 1 and 2, the observed variation of the Martian ionospheric peak height is correlated with three orbit parameters: latitude, local time and solar longitude. The latitude ranges of EDS1 and EDS2 are 60°N–85°N. The local time varies from ~03:00 (the northern summer) to ~07:00 (the northern autumn) for EDS1 and from ~04:00 (the northern summer) to ~14:00 (the northern autumn) for EDS2. The local time difference is as much as ~10 h. The solar longitudes vary from ~80° to ~200°. The variation of the neutral atmosphere caused by these three parameters is the possible reason for the increase in the subsolar ionospheric peak height from the northern summer to autumn. Figure 6 shows the variations of the neutral density at 130 km estimated by LMD MGCM model with latitude, local time and solar longitude. It is clear that the neutral density at 130 km varies with the three orbit parameter. However, it is difficult to separate the effect of each of the parameters on the neutral atmosphere.

[35] To investigate the expected variation of the Martian neutral atmosphere with latitude, local time and solar longitude, we retrieved LMD MGCM neutral density predictions at 20 km and 130 km above the equipotential surface at three local times (04:00, 08:00, 14:00) and at three latitudes (60°, 70°, 80°) with the same longitudes and solar longitudes as EDS1 under the solar maximum condition. The solar longitude variations of the estimated neutral densities at 20 km and 130 km and the derived effective neutral scale height between 20 km and 130 km are shown in Figure 7.

[36] The LMD MGCM model predictions verify that the latitude variations of the neutral atmospheric parameters are not important for the increase in the ionospheric peak height. The local time variation of the neutral density in the lower atmosphere of Mars (20 km above the equipotential surface) is negligible, which is in accord with the MGS/RS atmospheric measurement as shown in Figure 3. In comparison, the simulated neutral densities at 130 km at different local times show a clear solar longitude variation.

[37] An interesting feature shown in Figure 7 is the seasonal dependence of the local time variation in the neutral density at 130 km. It can be seen that the local time variations of the neutral density in the upper atmosphere and hence the effective neutral scale height becomes larger especially for the solar longitudes larger than 130°. The increase in $\overline{\xi}_{n-LMD}$ from LT = 4:00 to LT = 14:00 near the northern autumn is comparable with that caused by the solar longitude variation.

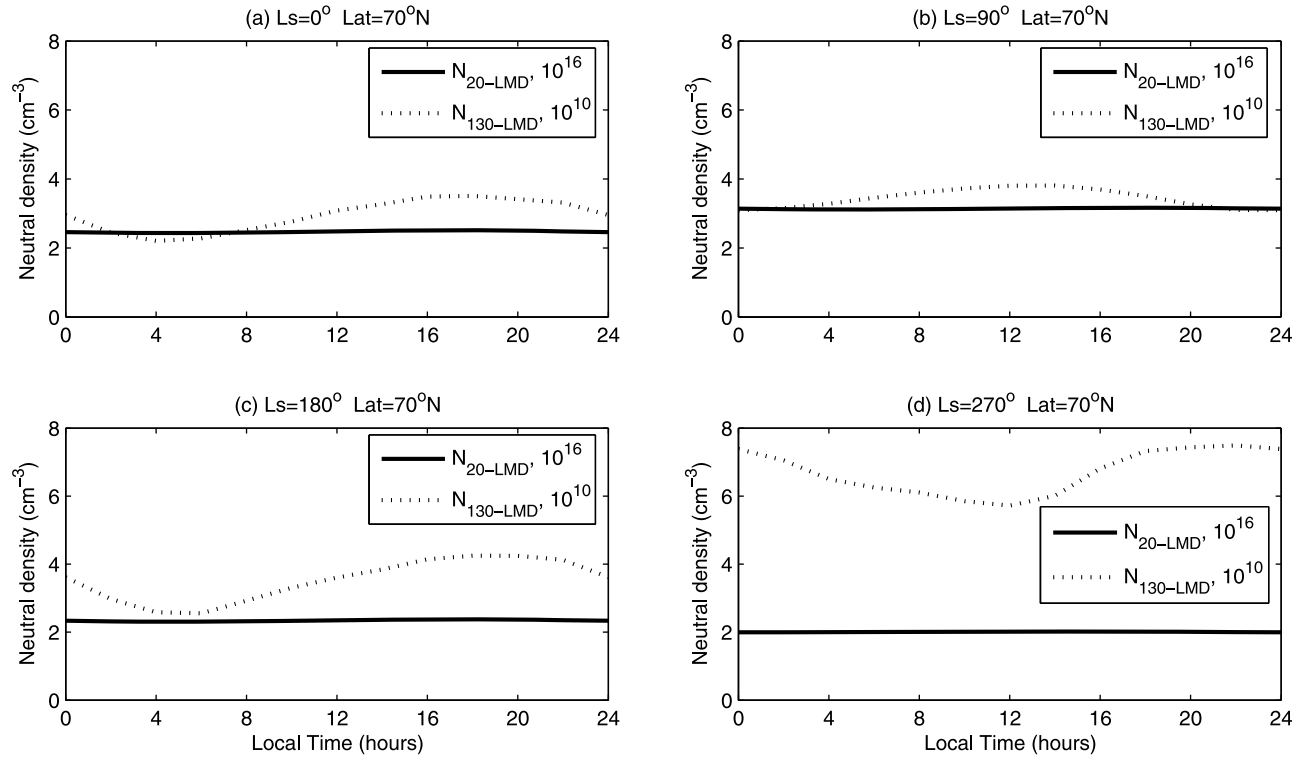

Figure 8. The local time variations of the neutral densities at 20 km and 130 km in four seasons. The neutral densities are simulated by the LMD MGCM model at Lat = 70°N and averaged over all longitudes to minimize the possible longitude variation. Four panels show the results at (a) Ls = 0°, (b) Ls = 90°, (c) Ls = 180° and (d) Ls = 270°. The solid line shows the neutral density at 20 km. The dotted line shows the neutral density at 130 km.

To examine this more closely, we examined the local time variations of the neutral densities predicted at 20 km and 130 km in different seasons with the LMD MGCM model. Figure 8 shows the local time variations of the longitudinal averaged neutral densities at 20 km and 130 km at Ls = 0°, 90°, 180° and 270°. The neutral densities are simulated at Lat = 70°N and averaged over all longitudes. It can be seen that the local time variations of the neutral density at 20 km in four seasons are negligible, while those of the neutral density at 130 km are quite different. Two similar local time variations are shown at two equinoxes, in which a density minimum appears at LT = 04:00 to 06:00 and a density maximum appears at LT = 16:00 to 18:00. However, the local time variations at two solstices show an opposite trend. The neutral density at 130 km shows a maximum at LT = 12:00 and a minimum at LT = 00:00/24:00 at the northern summer solstice (Ls = 90°). On the contrary, a density minimum is found at LT = 12:00 and a density maximum is found at LT = 00:00/24:00 at the northern winter solstice (Ls = 270°). This difference in diurnal density variations at the 2 solstices is not surprising given the 45% difference in global solar flux and resulting differences in general circulation.

[38] From Figures 1 and 2, it can be seen that the local time increases from ~4:00 in the northern summer to ~14:00 in the northern autumn for EDS2. From Figure 8, we can see that the relative variation of the neutral density at 130 km from LT = 04:00 to LT = 14:00 at Ls = 180° is much larger than that at Ls = 90°. Therefore the local time and solar longitude variations are both likely responsible for the increase in the ionospheric peak height of EDS2. However, the average local time difference of EDS1 is only ~4 h, increasing from LT = ~03:00 in the northern summer to ~07:00 in the northern autumn. From Figure 8, the local time variation of the neutral density at 130 km from LT = ~03:00 to LT = ~07:00 is negligible at Ls = 180°. Therefore the variations in ionospheric peak height for EDS1 are likely mostly due to variation in solar longitude. As mentioned above, the local time variation of the Martian upper atmospheric density also depends on seasons. Therefore the increase in the subsolar ionospheric peak from the northern summer (Ls = 90°) to the northern autumn (Ls = 180°) is believed to be mainly caused by the solar longitude variation of the neutral atmosphere below the ionospheric peak.

[39] The likely primary mechanism responsible for the solar longitude variations of the neutral density in the Mars upper atmosphere and the effective neutral scale height below the ionospheric peak is the change in subsolar latitude (SSL) from 25°N (northern summer, Ls = 90°) to the equator (northern autumn equinox, Ls = 180°). In general, the steady southward drift in SSL can cause the temperatures in the lower atmosphere to drop significantly at high northern latitudes. According to the MGS/RS neutral atmosphere measurements [*Hinson*, 2006], the surface temperature at high northern latitudes decreases from about 215 K at Ls = 90° to 175 K at Ls = 180°. Similarly, the neutral scale height at 20 km at high northern latitudes derived from the same measurements [*Zou et al.*, 2005] shows a 40% decrease

from northern summer to northern autumn equinox. Recent observations by the Mars Climate Sounder (MCS) on the Mars Reconnaissance Orbit (MRO) [*McCleese et al.*, 2010] verify this seasonal variation in Martian atmospheric temperatures at high northern latitudes from the surface to about 20 km. This decrease in temperature causes the contraction of the atmosphere below 20 km, which results in the decrease in neutral density at 20 km. However, the southward drift in SSL has the opposite effect on the temperatures at higher altitudes. The southward drift in SSL drives the seasonal evolution of the interhemispheric Hadley circulation, which becomes stronger as heliocentric distance decreases and the average atmospheric temperature increases from northern summer to northern autumn. Strong meridional winds lead to a horizontal convergence of mass and downward motion above the polar regions, resulting in adiabatic heating and polar warming. Generally, the effective neutral scale height studied here is determined by the neutral atmospheric temperature from 20 km to the ionospheric peak height. Therefore the polar warming in the lower and middle atmosphere is more important for this case. Lower and middle atmosphere (25–80 km) north polar warming has been reported [*Deming et al.*, 1986; *Jakosky and Martin*, 1987; *Théodore et al.*, 1993; *M. D. Smith et al.*, 2001] and simulated [*Wilson*, 1997; *Forget et al.*, 1999; *Bougher et al.*, 2006; *Hartogh et al.*, 2007; *González-Galindo et al.*, 2009] for several events. The north polar warming is shown to be most pronounced during perihelion conditions (Ls = 270°), when maximum solar insolation and strong dust heating prevail.

[40] However, recent observations by MCS on MRO showed that polar warming occurs in all seasons and the polar warming in the middle atmosphere (40 ~ 80 km) at high north latitudes becomes more intensive from northern summer to northern autumn (MY 29) [*McCleese et al.*, 2010]. Therefore the solar longitude variations of the lower and upper atmosphere can be explained by the southward drift in SSL. According to the MCS observations in MY 29, the middle atmospheric polar warming at the northern autumn equinox (Ls = 180°) is more intensive than that at the northern vernal equinox (Ls = 0°). Therefore, the change in the heliocentric distance of Mars plays an indirect role. We can rule out dust activity as a contributing factor to the thermosphere density increase since the data do not fall during the storm season (southern summer) and indeed there was little to no dust activity at this time [*Smith*, 2004].

8. Conclusion

[41] In this paper, we investigate long-term ionospheric and atmospheric measurements by the MGS/RS experiment. We find that the subsolar-equivalent peak heights of the Marian ionosphere at high north latitudes have a clear seasonal dependence, increasing from the northern summer (Ls = 90°) to the northern autumn (Ls = 180°). This is a direct result of the seasonal variation of the neutral atmosphere below the ionospheric peak. Predictions from the LMD MGCM model confirm this seasonal variation in 91) the neutral atmospheric density at the ionospheric peak and 92) the effective neutral scale height between the reference height (20 km) and the ionospheric peak height.

[42] We believe the primary mechanism responsible for the seasonal variation of the neutral atmosphere below the ionospheric peak, in the high northern latitudes, from northern summer to northern autumn, to be the southward drift in subsolar latitude and (to a lesser extent) decreasing heliocentric distance, which drives the seasonal evolution of the interhemispheric Hadley circulation on Mars. The downward branch of this circulation leads to an increasing polar warming in the middle atmosphere at high north latitudes from the northern summer to the northern autumn, causing an increase in neutral scale height at and below the ionospheric peak. This explains the northern summer-autumn increase in the ionospheric peak height.

[43] **Acknowledgments.** We thank the MGS Radio Science Team for making their ionosphere and neutral atmosphere profile data available on a public Web site. We also thank the LMD group in Paris for providing the Mars Climate Database. This research was funded by National Science Foundation of China (grants 40704026 and 40931056) and the foundation of Co-construction of Beijing Municipal Commission of Education 25 (grant XK100010404), as well as NASA Mars Data Analysis Program grant NNX07AV42G.

References

Angelats i Coll, M., F. Forget, M. A. López-Valverde, P. L. Read, and S. Lewis (2004), Upper atmosphere of Mars up to 120 km: Mars Global Surveyor data analysis with the LMD general circulation model, *J. Geophys. Res.*, *109*, E01011, doi:10.1029/2003JE002163.

Angelats i Coll, M., F. Forget, M. A. López-Valverde, and F. Gonzalez-Galindo (2005), The first Mars thermospheric general circulation model: The Martian atmosphere from the ground to 240 km, *Geophys. Res. Lett.*, *32*, L04201, doi:10.1029/2004GL021368.

Bauer, S. J., and M. H. Hantsch (1989), Solar cycle variation of the upper atmosphere temperature of Mars, *Geophys. Res. Lett.*, *16*, 373–376, doi:10.1029/GL016i005p00373.

Bougher, S. W., R. G. Roble, E. C. Ridley, and R. E. Dickinson (1990), The Mars thermosphere: 2. General circulation with coupled dynamics and composition, *J. Geophys. Res.*, *95*, 14,811–14,827, doi:10.1029/JB095iB09p14811.

Bougher, S. W., S. Engel, R. G. Roble, and B. Foster (1999), Comparative terrestrial planet thermospheres: 2. Solar cycle variation of global structure and winds at equinox, *J. Geophys. Res.*, *104*, 16,591–16,611, doi:10.1029/1998JE001019.

Bougher, S. W., S. Engel, R. G. Roble, and B. Foster (2000), Comparative terrestrial planet thermospheres: 3. Solar cycle variation of global structure and winds at solstices, *J. Geophys. Res.*, *105*, 17,669–17,692, doi:10.1029/1999JE001232.

Bougher, S. W., S. Engel, D. P. Hinson, and J. M. Forbes (2001), Mars Global Surveyor Radio Science electron density profiles: Neutral atmosphere implications, *Geophys. Res. Lett.*, *28*, 3091–3094, doi:10.1029/2001GL012884.

Bougher, S. W., S. Engel, D. P. Hinson, and J. R. Murphy (2004), MGS Radio Science electron density profiles: Interannual variability and implications for the Martian neutral atmosphere, *J. Geophys. Res.*, *109*, E03010, doi:10.1029/2003JE002154.

Bougher, S. W., J. M. Bell, J. R. Murphy, M. A. Lopez-Valverde, and P. G. Withers (2006), Polar warming in the Mars thermosphere: Seasonal variations owing to changing insolation and dust distributions, *Geophys. Res. Lett.*, *33*, L02203, doi:10.1029/2005GL024059.

Breus, T. K., A. M. Krymskii, D. H. Crider, N. F. Ness, D. Hinson, and K. K. Barashyan (2004), Effect of the solar radiation in the topside atmosphere/ionosphere of Mars: Mars Global Surveyor observations, *J. Geophys. Res.*, *109*, A09310, doi:10.1029/2004JA010431.

Budden, K. G. (1966), *Radio Waves in the Ionosphere*, Cambridge Univ. Press, London.

Cahoy, K. L., D. P. Hinson, and G. L. Tyler (2006), Radio science measurements of atmospheric refractivity with Mars Global Surveyor, *J. Geophys. Res.*, *111*, E05003, doi:10.1029/2005JE002634.

Cahoy, K. L., D. P. Hinson, and G. L. Tyler (2007), Characterization of a semidiurnal eastward-propagating tide at high northern latitudes with Mars Global Surveyor electron density profiles, *Geophys. Res. Lett.*, *34*, L15201, doi:10.1029/2007GL030449.

Chapman, S. (1931), The absorption and dissociative or ionizing effects of monochromatic radiation in an atmosphere of a rotating Earth. Part II. Grazing incidence, *Proc. Phys. Soc. London*, *43*, 483–501, doi:10.1088/0959-5309/43/5/302.

Clancy, R. T., S. J. Sandor, M. J. Wolff, P. R. Christensen, M. D. Smith, J. C. Pearl, B. J. Conrath, and R. J. Wilson (2000), An intercomparison of ground-based millimeter, MGS TES, and Viking atmospheric temperature measurements: Seasonal and interannual variability of temperatures and dust loading in the global Mars atmosphere, *J. Geophys. Res.*, *105*, 9553–9571, doi:10.1029/1999JE001089.

Deming, D., M. J. Mumma, F. Espenak, and T. Kostiuk (1986), Polar warming in the middle atmosphere of Mars, *Icarus*, *66*, 366–379, doi:10.1016/0019-1035(86)90165-X.

Fjeldbo, G., D. Sweetham, J. Brenkle, E. Christensen, D. Farless, J. Mehta, B. Seidel, W. Michael Jr., A. Wallio, and M. Grossi (1977), Viking radio occultation measurements of the Martian atmosphere and topography: Primary mission coverage, *J. Geophys. Res.*, *82*, 4317–4324, doi:10.1029/JS082i028p04317.

Forget, F., F. Hourdin, R. Fournier, C. Hourdin, O. Talagrand, M. Collins, S. R. Lewis, P. L. Read, and J.-P. Huot (1999), Improved general circulation models of the Martian atmosphere from the surface to above 80 km, *J. Geophys. Res.*, *104*, 24,155–24,175, doi:10.1029/1999JE001025.

Forget, F., F. Montmessin, J.-L. Bertaux, F. González-Galindo, S. Lebonnois, E. Quémerais, A. Reberac, E. Dimarellis, and M. A. López-Valverde (2009), Density and temperatures of the upper Martian atmosphere measured by stellar occultations with Mars Express SPICAM, *J. Geophys. Res.*, *114*, E01004, doi:10.1029/2008JE003086.

Fox, J. L., and K. E. Yeager (2006), Morphology of the near-terminator Martian ionosphere: A comparison of models and data, *J. Geophys. Res.*, *111*, A10309, doi:10.1029/2006JA011697.

Fox, J. L., and K. E. Yeager (2009), MGS electron density profiles: Analysis of the peak magnitudes, *Icarus*, *200*, 468–479, doi:10.1016/j.icarus.2008.12.002.

González-Galindo, F., M. A. López-Valverde, M. Angelats i Coll, and F. Forget (2005), Extension of a Martian GCM to thermospheric altitudes: UV heating and photochemical models, *J. Geophys. Res.*, *110*, E09008, doi:10.1029/2004JE002312.

González-Galindo, F., F. Forget, M. A. López-Valverde, and M. Angelats i Coll (2009), A ground-to-exosphere Martian general circulation model: 2. Atmosphere during solstice conditions—Thermospheric polar warming, *J. Geophys. Res.*, *114*, E08004, doi:10.1029/2008JE003277.

Gurnett, D. A., et al. (2005), Radar soundings of the ionosphere of Mars, *Science*, *310*, 1929–1933, doi:10.1126/science.1121868.

Hantsch, M. H., and S. J. Bauer (1990), Solar control of the Mars ionosphere, *Planet Space Sci.*, *38*, 539–542, doi:10.1016/0032-0633(90)90146-H.

Hartogh, P., A. S. Medvedev, and C. Jarchow (2007), Middle atmosphere polar warmings on Mars: Simulations and study on the validation with sub-millimeter observations, *Planet. Space Sci.*, *55*, 1103–1112, doi:10.1016/j.pss.2006.11.018.

Hinson, D. P. (2006), Radio occultation measurements of transient eddies in the northern hemisphere of Mars, *J. Geophys. Res.*, *111*, E05002, doi:10.1029/2005JE002612.

Hinson, D. P. (2008a), Mars Global Surveyor Radio Occultation Profiles of the Ionosphere: Reorganized, MGS-M-RSS-5-EDS-V1.0, http://starbrite.jpl.nasa.gov/pds/viewProfile.jsp?dsid=MGS-M-RSS-5-EDS-V1.0, NASA Planet. Data Syst., Washington, D. C.

Hinson, D. P. (2008b), Mars Global Surveyor Radio Occultation Profiles of the Neutral Atmosphere: Reorganized, MGS-M-RSS-5-TPS-V1.0, http://starbrite.jpl.nasa.gov/pds/viewDataset.jsp?dsid=MGS-M-RSS-5-TPS-V1.0, NASA Planet. Data Syst., Washington, D. C.

Hinson, D. P., R. A. Simpson, J. D. Twicken, G. L. Tyler, and F. M. Flasar (1999), Initial results from radio occultation measurements with Mars Global Surveyor, *J. Geophys. Res.*, *104*, 26,997–27,012, doi:10.1029/1999JE001069.

Jakosky, B. M., and T. Z. Martin (1987), Mars: North polar atmospheric warming during dust storms, *Icarus*, *72*, 528–534, doi:10.1016/0019-1035(87)90050-9.

Keating, G. M., et al. (1998), The structure of the upper atmosphere of mars: In situ accelerometer measurements from Mars Global Surveyor, *Science*, *279*, 1672–1676, doi:10.1126/science.279.5357.1672.

Krymskii, A. M., T. K. Breus, and E. Nielsen (1995), On possible observational evidence in electron density profiles of a magnetic field in the Martian ionosphere, *J. Geophys. Res.*, *100*, 3721–3730, doi:10.1029/94JA03005.

Krymskii, A. M., T. K. Breus, N. F. Ness, M. H. Acuña, J. E. P. Connerney, D. H. Crider, D. L. Mitchell, and S. J. Bauer (2002), Structure of the magnetic field fluxes connected with crustal magnetization and topside ionosphere at Mars, *J. Geophys. Res.*, *107*(A9), 1245, doi:10.1029/2001JA000239.

Krymskii, A. M., T. K. Breus, N. F. Ness, D. P. Hinson, and D. I. Bojkov (2003), Effect of crustal magnetic fields on the near terminator ionosphere at Mars: Comparison of in situ magnetic field measurements with the data of radio science experiments on board Mars Global Surveyor, *J. Geophys. Res.*, *108*(A12), 1431, doi:10.1029/2002JA009662.

Krymskii, A. M., N. F. Ness, D. H. Crider, T. K. Breus, M. H. Acuña and D. P. Hinson (2004), Solar wind interaction with the ionosphere/atmosphere and crustal magnetic fields at Mars: Mars Global Surveyor Magnetometer/Electron Reflectometer, radio science, and accelerometer data, *J. Geophys. Res.*, *109*, A11306, doi:10.1029/2004JA010420.

Lefèvre, F., S. Lebonnois, F. Montmessin, and F. Forget (2004), Three-dimensional modeling of ozone on Mars, *J. Geophys. Res.*, *109*, E07004, doi:10.1029/2004JE002268.

Lillis, R. J., S. W. Bougher, F. González-Galindo, F. Forget, M. D. Smith, and P. C. Chamberlin (2010), Four Martian years of nightside upper thermospheric mass densities derived from electron reflectometry: Method extension and comparison with GCM simulations, *J. Geophys. Res.*, *115*, E07014, doi:10.1029/2009JE003529.

Lindal, G. F., H. B. Hotz, D. N. Sweetnam, Z. Shippony, J. P. Brenkle, G. V. Hartsell, R. T. Spear, and W. H. Michael Jr. (1979), Viking radio occultation measurements of the atmosphere and topography of Mars: Data acquired during 1 Martian year of tracking, *J. Geophys. Res.*, *84*, 8443–8456, doi:10.1029/JB084iB14p08443.

Liu, J., M. I. Richardson, and R. J. Wilson (2003), An assessment of the global, seasonal, and interannual spacecraft record of Martian climate in the thermal infrared, *J. Geophys. Res.*, *108*(E8), 5089, doi:10.1029/2002JE001921.

McCleese, D. J., et al. (2010), Structure and dynamics of the Martian lower and middle atmosphere as observed by the Mars Climate Sounder: Seasonal variations in zonal mean temperature, dust, and water ice aerosols, *J. Geophys. Res.*, *115*, E12016, doi:10.1029/2010JE003677.

Millour, E., et al. (2008), The latest (version 4.3) Mars Climate Database, paper presented at Third International Workshop on The Mars Atmosphere: Modeling and Observations, Lunar and Planet. Inst., Williamsburg, Va., 10–13 Nov.

Montmessin, F., F. Forget, P. Rannou, M. Cabane, and R. M. Haberle (2004), Origin and role of water ice clouds in the Martian water cycle as inferred from a general circulation model, *J. Geophys. Res.*, *109*, E10004, doi:10.1029/2004JE002284.

Morgan, D. D., D. A. Gurnett, D. L. Kirchner, J. L. Fox, E. Nielsen, and J. J. Plaut (2008), Variation of the Martian ionospheric electron density from Mars Express radar soundings, *J. Geophys. Res.*, *113*, A09303, doi:10.1029/2008JA013313.

Nielsen, E., et al. (2007), Local plasma processes and enhanced electron densities in the lower ionosphere in magnetic cusp regions on Mars, *Planet. Space Sci.*, *55*, 2164–2172, doi:10.1016/j.pss.2007.07.003.

Seiff, A., and D. B. Kirk (1976), Structure of Mars' atmosphere up to 100 kilometers from the entry measurements of Viking 2, *Science*, *194*, 1300–1303, doi:10.1126/science.194.4271.1300.

Smith, D. E., et al. (2001), Mars Orbiter Laser Altimeter: Experiment summary after the first year of global mapping of Mars, *J. Geophys. Res.*, *106*, 23,689–23,722, doi:10.1029/2000JE001364.

Smith, M. D. (2004), Interannual variability in TES atmospheric observations of Mars during 1999–2003, *Icarus*, *167*, 148–165, doi:10.1016/j.icarus.2003.09.010.

Smith, M. D., J. C. Pearl, B. J. Conrath, and P. R. Christensen (2001), Thermal Emission Spectrometer results: Atmospheric thermal structure and aerosol distribution, *J. Geophys. Res.*, *106*, 23,929–23,945, doi:10.1029/2000JE001321.

Stewart, A. I., and W. B. Hanson (1982), Mars upper atmosphere: Mean and variations, *Adv. Space Res.*, *2*, 87–101, doi:10.1016/0273-1177(82)90109-0.

Théodore, B., et al. (1993), Solstial temperature inversions in the Martian middle atmosphere: Observational clues and 2-D modeling, *Icarus*, *105*, 512–528, doi:10.1006/icar.1993.1145.

Titheridge, J. E. (1988), An approximate form for the Chapman grazing incidence function, *J. Atmos. Terr. Phys.*, *50*, 699–701, doi:10.1016/0021-9169(88)90033-5.

Torr, M. R., D. G. Torr, and R. A. Ong (1979), Ionization frequencies for major thermospheric constituents as a function of solar cycle 21, *Geophys. Res. Lett.*, *6*, 771–774, doi:10.1029/GL006i010p00771.

Wang, J.-S., and E. Nielsen (2003), Behavior of the Martian dayside electron density peak during global dust storms, *Planet. Space Sci.*, *51*, 329–338, doi:10.1016/S0032-0633(03)00015-1.

Wang, J.-S., and E. Nielsen (2004), Evidence for topographic effects on the Martian ionosphere, *Planet. Space Sci.*, *52*, 881–886, doi:10.1016/j.pss.2004.01.008.

Wilson, R. J. (1997), A general circulation model of the Martian polar warming, *Geophys. Res. Lett.*, *24*, 123–126, doi:10.1029/96GL03814.

Withers, P. (2006), Mars Global Surveyor and Mars Odyssey Accelerometer observations of the Martian upper atmosphere during aerobraking, *Geophys. Res. Lett.*, *33*, L02201, doi:10.1029/2005GL024447.

Withers, P. (2009), A review of observed variability in the dayside ionosphere of Mars, *Adv. Space Res.*, *44*, 277–307, doi:10.1016/j.asr.2009.04.027.

Withers, P., S. W. Bougher, and G. M. Keating (2003), The effects of topographically controlled thermal tides in the Martian upper atmosphere as seen by the MGS accelerometer, *Icarus*, *164*, 14–32, doi:10.1016/S0019-1035(03)00135-0.

Withers, P., M. Mendillo, D. P. Hinson, and K. Cahoy (2008), Physical characteristics and occurrence rates of meteoric plasma layers detected in the Martian ionosphere by the Mars Global Surveyor Radio Science Experiment, *J. Geophys. Res.*, *113*, A12314, doi:10.1029/2008JA013636.

Zhang, M. H. G., J. G. Luhmann, A. J. Kliore, and J. Kim (1990), A post-pioneer Venus reassessment of the Martian dayside ionosphere as observed by radio occultation methods, *J. Geophys. Res.*, *95*, 14,829–14,839, doi:10.1029/JB095iB09p14829.

Zou, H., J.-S. Wang, and E. Nielsen (2005), Effect of the seasonal variations in the lower atmosphere on the altitude of the ionospheric main peak at Mars, *J. Geophys. Res.*, *110*, A09311, doi:10.1029/2004JA010963.

Zou, H., J.-S. Wang, and E. Nielsen (2006), Reevaluating the relationship between the Martian ionospheric peak density and the solar radiation, *J. Geophys. Res.*, *111*, A07305, doi:10.1029/2005JA011580.

Zou, H., H. F. Chen, N. Yu, W. H. Shi, X. Q. Yu, J. Q. Zou, and W. Y. Zhong (2010), Effects of Martian crustal magnetic field on its ionosphere, *Sci. China Tech. Sci.*, *53*, 1717–1724, doi:10.1007/s11431-010-3118-1.

Zwillinger, D. (1992), *Handbook of Integration*, Jones and Bartlett, Boston, Mass.

R. J. Lillis, Space Science Laboratory, University of California, 7 Gauss Way, Berkeley, CA 94720, USA.

E. Nielsen, Max Planck Institute for Solar System Research, Max Planck Str. 2, D-37191 Katlenburg-Lindau, Germany.

J. S. Wang, National Center for Space Weather, China Meteorological Administration, Beijing 100081, China.

H. Zou, Institute of Space Physics and Applied Technology, School of Earth and Space Sciences, Peking University, Beijing 100871, China. (derakzou@yahoo.com.cn)